The Meteoritical Society

Meteoritics & Planetary Science 44, Nr 11, 1771–1786 (2009)
Abstract available online at http://meteoritics.org

Transformation textures, mechanisms of formation of high-pressure minerals in shock melt veins of L6 chondrites, and pressure-temperature conditions of the shock events

Shin OZAWA[1*], Eiji OHTANI[1], Masaaki MIYAHARA[1], Akio SUZUKI[1], Makoto KIMURA[2], and Yoshinori ITO[1]

[1]Department of Earth and Planetary Materials Science, Graduate School of Science, Tohoku University, Sendai 980–8578, Japan
[2]Faculty of Science, Ibaraki University, Mito 310-8512, Japan
[*]Corresponding author. E-mail: shin-ozawa@m.tains.tohoku.ac.jp

(Received 30 December 2008; revision accepted 25 July 2009)

Abstract–The high-pressure polymorphs of olivine, pyroxene, and plagioclase in or adjacent to shock melt veins (SMVs) in two L6 chondrites (Sahara 98222 and Yamato 74445) were investigated to clarify the related transformation mechanisms and to estimate the pressure-temperature conditions of the shock events. Wadsleyite and jadeite were identified in Sahara 98222. Wadsleyite, ringwoodite, majorite, akimotoite, jadeite, and lingunite ($NaAlSi_3O_8$-hollandite) were identified in Yamato 74445. Wadsleyite nucleated along the grain boundaries and fractures of original olivine. The nucleation and growth of ringwoodite occurred along the grain boundaries of original olivine, and as intracrystalline ringwoodite lamellae within original olivine. The nucleation and growth of majorite took place along the grain boundaries or fractures in original enstatite. Jadeite-containing assemblages have complicated textures containing "particle-like," "stringer-like," and "polycrystalline-like" phases. Coexistence of lingunite and jadeite-containing assemblages shows a vein-like texture. We discuss these transformation mechanisms based on our textural observations and chemical composition analyses. The shock pressure and temperature conditions in the SMVs of these meteorites were also estimated based on the mineral assemblages in the SMVs and in comparison with static high-pressure experimental results as follows: 13–16 GPa, >1900 °C for Sahara 98222 and 17–24 GPa, >2100 °C for Yamato 74445.

INTRODUCTION

High-pressure phase transformations of minerals occur in the deep interior of terrestrial planets or in shock-metamorphosed rocks (including meteorites) induced by the collisions of planetary bodies. Knowledge of the mechanisms of high-pressure phase transformations for rock-forming minerals is important to understand the dynamics and processes of planetary interiors, such as slab subduction, mantle convection, mantle rheology, and the genesis of deep-focus earthquakes (e.g., Sung and Burns 1976; Rubie 1984; Rubie and Ross 1994; Kirby et al. 1996; Riedel and Karato 1997; Karato et al. 2001). High-pressure and high–temperature experiments on the major constituent minerals of the Earth (e.g., olivine, pyroxene, and feldspar) have been carried out to clarify the kinetics of their phase transformations (e.g., Brearley et al. 1992; Hogrefe et al. 1994; Rubie and Ross 1994; Kerschhofer et al. 1996, 2000; Kubo et al. 1998, 2004, 2008; Mosenfelder et al. 2000, 2001). The observation and description of naturally transformed samples are necessary to ascertain whether the transformation mechanism observed in the experiments could actually occur in nature. The opportunity for the investigation of natural high-pressure phase transformations is limited to a few samples, such as diamond inclusions derived from ultra-deep mantle, or rocks naturally shocked in planetary impacts. Among these, heavily shocked meteorites are unique and important samples because they contain many different high-pressure minerals. Heavily shocked meteorites contain pervasive shock melt veins (SMVs) or melt pockets, where many high-pressure minerals have been discovered (e.g., Sharp and DeCarli 2006; Gillet et al. 2007).

Another aspect of shocked meteorites is that they provide us with information about the impact processes on their parent bodies. Many shock-recovery experiments have been carried out to evaluate the effects of shock metamorphism on rocks under various pressure conditions (e.g., Stöffler et al. 1991; Schmitt 2000; Xie et al. 2001a). For example, Stöffler et al. (1991) compared shock features observed in experimentally shocked samples with those of shocked chondrites, and

developed a shock classification scheme (Shock stage S1–S6). This classification has been widely used to evaluate the degree of shock metamorphism, and to calibrate shock pressures experienced by natural samples. However, there are some problems, as the time scale of shock compression in experiments (at the order of 10^{-9}–10^{-6} seconds) is much shorter than that of natural planetary impact processes (at the order of 10^{-3}–10^{0} seconds). Dynamic experiments have not succeeded in producing most of the high-pressure phases observed in shocked meteorites. On the other hand, static high-pressure experiments involve comparatively longer duration high-pressure and high-temperature conditions (typically at the order of 10^{0}–10^{3} seconds) than shock experiments. Recovered samples of static melting experiments on Allende CV chondrite and KLB1 peridotite (e.g., Zhang and Herzberg 1994; Agee et al. 1995; Asahara et al. 2004) show similarities with the SMVs of chondrites in terms of high-pressure phase assemblages, grain size, and chemical composition. Thus, it seems appropriate to compare with static high-pressure experimental results when discussing the kinetic features in meteorites, such as the high-pressure phase transformations.

The aim of this study was to investigate the natural transformation textures of high-pressure minerals in the SMVs of two L6 chondrites (Sahara 98222 and Yamato 74445) and elucidate the mechanisms of the phase transformations. We also estimated the pressure and temperature conditions of these chondrites during the impact events, based on the mineral assemblages in the SMVs and their pressure-temperature stability fields determined from static high-pressure experimental data.

MATERIALS AND EXPERIMENTAL PROCEDURE

The Sahara 98222 chondrite was found in 1998 in the Sahara and is classified as an L6 chondrite (Grossman 1999). Grossman (1999) reported that Sahara 98222 contains ringwoodite, and its shock stage was determined as S6. The Yamato 74445 chondrite was found in Antarctica in 1974 and is classified as an L6 chondrite (Yanai and Kojima 1995). Yanai and Kojima (1995) reported that Yamato 74445 contains maskelynite, shock-induced feldspar glass. Its shock stage has not yet been determined.

We studied several petrographic thin sections of Sahara 98222 and Yamato 74445 chondrites containing SMVs. The petrological and mineralogical textures of the samples were observed using optical microscopes with transmitted and reflected light. Fine textures of the high-pressure minerals were investigated using a JEOL-71010 field emission scanning electron microscope (FE-SEM). The accelerating voltage and electron beam current used were 15 kV and around 1 nA, respectively. Phase identification of minerals was conducted using a JASCO NRS-2000 laser micro-Raman spectrometer (Ar^{+} laser, 514.5 and 488.0 nm lines). The laser power used was 12–20 mW, and the size of the laser beam was ~1 μm in diameter. The Raman spectra of the minerals were collected for a period of 30–600 s, and accumulated twice. The chemical composition of the minerals was determined using a JEOL JXA8800M electron probe micro-analyzer (EPMA) with a wavelength dispersive X-ray spectrometer (WDS). The accelerating voltage and electron beam current used were 15 kV and 3–20 nA, respectively (~12 nA for olivine and its polymorphs, 15–20 nA for pyroxene and its polymorphs, and 3–11 nA for plagioclase and its polymorphs). The probe diameter was 1–15 μm. When we analyzed the chemical composition of lingunite ($NaAlSi_3O_8$-hollandite) in Yamato 74445, which was very sensitive to volatilization by the electron beam, a dedicated stage cooled with liquid nitrogen was used to prevent any damage from the electron beam during the measurements. The standards used were as follows: forsterite (Mg_2SiO_4) for Mg and Si, fayalite (Fe_2SiO_4) for Fe, wollastonite ($CaSiO_3$) for Ca, Al_2O_3 for Al, jadeite ($NaAlSi_2O_6$) for Na, adularia ($KAlSi_3O_8$) for K, TiO_2 for Ti, Cr_2O_3 for Cr, Mn_2SiO_4 for Mn, and NiO for Ni.

RESULTS

Overview of the Shock Metamorphic Features

The Sahara 98222 and Yamato 74445 chondrites consist of host rock and pervasive SMVs (Fig. 1). The major constituent minerals of the host rock are olivine (Fo_{76}), enstatite (En_{79}), diopside ($En_{48}Fs_8Wo_{44–45}$), plagioclase ($Ab_{83–85}An_{10}Or_{5–7}$), metallic iron-nickel, and troilite, with minor amounts of phosphates (Table 1). Olivine and pyroxene show typical shock metamorphic features, such as undulatory extinction, irregular fractures, and sets of planar fractures. Most of the plagioclase has been transformed to maskelynite, a shock-induced diaplectic glass. The shock features observed, and the existence of wadsleyite and ringwoodite discussed later, indicate that both Sahara 98222 and Yamato 74445 should be classified as being of shock stage S6 (Stöffler et al. 1991).

Transformation Textures of High-Pressure Minerals in the SMVs of Sahara 98222

Pervasive SMVs with a width of 0.1–2.5 mm were observed in Sahara 98222 (Fig. 1). The SMVs consist of coarse-grained fragments of host rock and a fine-grained matrix filling inside the SMVs. We identified wadsleyite and jadeite as high-pressure minerals in the coarse-grained fragments embedded within the SMVs (Figs. 2, 3, and 7).

The original olivine grains have partially or totally transformed to the high-pressure polymorph wadsleyite (Figs. 2 and 7a). Back-scattered electron (BSE) images show that wadsleyite occurs as polycrystalline aggregates with up to

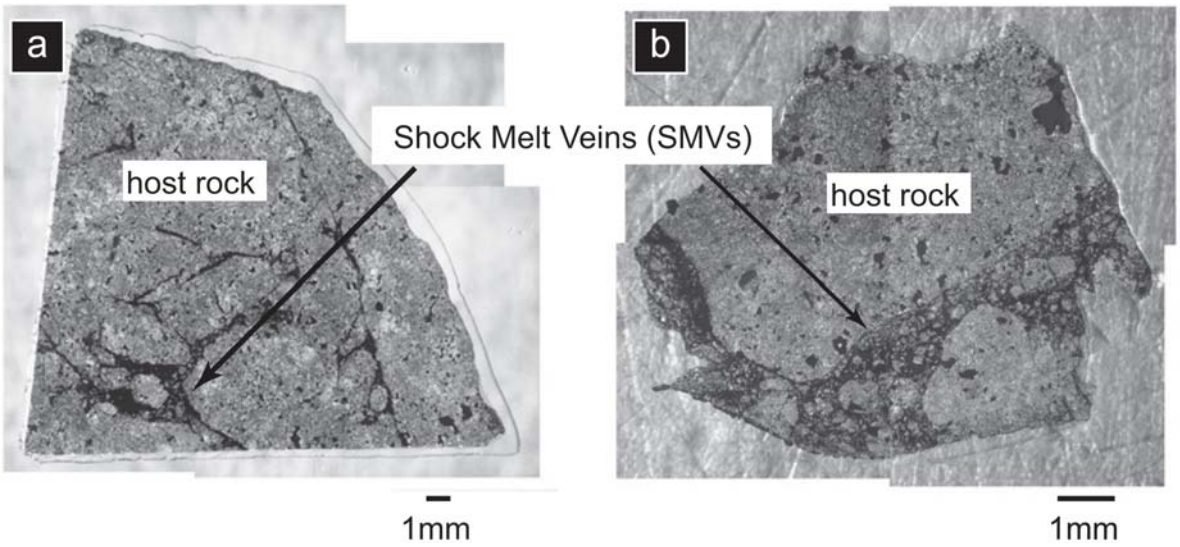

Fig. 1. Photomicrographs of the two samples under transmitted light. a) Sahara 98222 and b) Yamato 74445 L6 chondrites, both showing intricate networks of shock melt veins (SMVs).

~150 μm sizes. In partially transformed olivine grains, wadsleyite mainly exists along the margins of the original olivine adjacent to the matrix of the SMVs (Figs. 2a and 2b). The width of the wadsleyite aggregates is 3–30 μm. Individual wadsleyite crystals are granular or columnar and have sizes up to 10 μm. Wadsleyite also occurs along the margins of the original olivine grains, which are not in contact with the matrix of the SMVs (Figs. 2b and 2c). This wadsleyite also occurs as polycrystalline assemblages of up to 5 μm in size. Individual wadsleyite crystals have sizes up to 2 μm. We also identified wadsleyite along fractures in the original olivine grains (Fig. 2d). The chemical composition of the observed wadsleyite (Fo_{76}) is almost identical to that of the former olivine (Fo_{76}) (Table 1). In our Sahara 98222 section, we could not identify ringwoodite, which has been described from this meteorite in a previous report (Grossman 1999).

Jadeite was identified in grains that were originally plagioclase (Figs. 3 and 7b). BSE images show that jadeite-containing grains have quite complicated textures with numerous small "particle-like," "stringer-like," and "polycrystalline-like" phases, which have not been reported before. The diameter of the "particle-like" phase is up to 0.6 μm. The width and length of the "stringer-like" phase are around 0.5 μm and up to 20 μm, respectively. These two phases occur in the inner parts of the grains. In contrast, the "polycrystalline-like" phase is dominant along the margins of the grains adjacent to the matrix of the SMVs. Typical Raman peaks of jadeite (380, 440, 527, 579, 703, 990, and 1042 cm^{-1}) were detected from whole grains (Fig. 7b), and the intensity of the peaks was relatively higher at the grain margins (dominated by the "polycrystalline-like" phase) than in the grain interiors (dominated by the "particle-like" and the "stringer-like" phases). It was difficult to obtain the chemical composition of these phases because they are smaller than the diameter of the electron beam of the EPMA. Only the average composition was obtained by using a broad electron beam (Table 1). The bulk composition of the jadeite-containing grains ($Ab_{86}An_{10}Or_4$) is almost identical to that of maskelynite ($Ab_{85}An_{10}Or_4$), although the jadeite-containing grains have slightly higher Na and Fe concentrations. The higher Fe concentration in the jadeite-containing grains could be due to contamination by Fe-Ni-S inclusions. We did not see any significant Raman peaks of residual plagioclase (at 478 and 510 cm^{-1}) or a broad Raman signal from maskelynite (around 500, 590, 820, and 1100 cm^{-1}) in the jadeite-containing grains. Therefore, it is considered that these grains consist of jadeite crystallites plus an amorphous phase, and the chemical composition of the amorphous phase is "[original plagioclase]-[crystallized jadeite]." The chemical composition of the amorphous phase could be different from grain to grain, depending on the amounts of crystallized jadeite.

Transformation Textures of High-Pressure Minerals in the SMVs of Yamato 74445

SMVs with a width of 0.4–3.3 mm were observed in Yamato 74445 (Fig. 1). We identified ringwoodite, wadsleyite, majorite, akimotoite, jadeite, and lingunite ($NaAlSi_3O_8$-hollandite) as high-pressure minerals in the coarse-grained fragments in the SMVs or host rock adjacent to the SMVs (Figs. 4–7).

The original coarse-grained olivine grains in the SMVs or in host rock adjacent to the SMVs have been replaced by ringwoodite (Figs. 4 and 7c). We identified three different occurrences of ringwoodite. The first occurrence is ringwoodite crystallites nucleated along the grain margins of

Table 1. Chemical compositions of the minerals and glass in the Sahara 98222 L6 chondrite obtained using EPMA-WDS.

	Olivine		Wadsleyite		Enstatite		Diopside		Maskelynite		Jadeite	
n	9		6		8		10		8		6	
	Chemical composition (wt%)											
	av	σ	av	σ	av	σ	av	σ	av	σ	av	σ
SiO_2	38.54	0.26	38.60	0.46	55.94	0.32	54.16	0.19	65.86	0.41	65.55	0.50
TiO_2	n.d.	–	n.d.	–	0.18	0.02	0.43	0.02	–	–	–	–
Al_2O_3	n.d.	–	n.d.	–	0.15	0.02	0.46	0.03	21.42	0.28	21.36	0.28
Cr_2O_3	n.d.	–	n.d.	–	n.d.	–	0.86	0.10	–	–	–	–
FeO#	21.56	0.26	22.11	0.48	13.41	0.37	4.79	0.33	0.38	0.10	0.54	0.08
MnO	0.43	0.02	0.44	0.03	0.44	0.04	0.23	0.03	–	–	–	–
NiO	n.d.	–	n.d.	–	–	–	–	–	–	–	–	–
MgO	39.17	0.40	38.95	0.44	29.00	0.30	16.63	0.10	–	–	–	–
CaO	n.d.	–	n.d.	–	0.59	0.16	21.56	0.41	2.06	0.05	2.09	0.04
Na_2O	–	–	–	–	n.d.	–	0.54	0.04	9.49	0.09	9.71	0.15
K_2O	–	–	–	–	n.d.	–	n.d.	–	0.74	0.11	0.73	0.22
Total	99.71	0.44	100.10	0.45	99.71	0.37	99.66	0.37	99.95	0.41	99.98	0.54
	Cation formula											
Si	1.00	<0.01	1.00	<0.01	2.00	<0.01	1.99	<0.01	2.90	0.01	2.89	0.01
Ti	–	–	–	–	<0.01	<0.01	0.01	<0.01	–	–	–	–
Al	–	–	–	–	0.01	<0.01	0.02	<0.01	1.11	0.01	1.11	0.01
Cr	–	–	–	–	–	–	0.03	<0.01	–	–	–	–
Fe#	0.47	0.01	0.48	0.01	0.40	0.01	0.15	0.01	0.01	<0.01	0.02	<0.01
Mn	0.01	<0.01	0.01	<0.01	0.01	<0.01	0.01	<0.01	–	–	–	–
Ni	–	–	–	–	–	–	–	–	–	–	–	–
Mg	1.52	0.01	1.51	0.01	1.55	0.01	0.91	0.01	–	–	–	–
Ca	–	–	–	–	0.02	0.01	0.85	0.02	0.10	<0.01	0.10	<0.01
Na	–	–	–	–	–	–	0.04	<0.01	0.81	0.01	0.83	0.01
K	–	–	–	–	–	–	–	–	0.04	0.01	0.04	0.01
Total	3.00	<0.01	3.00	<0.01	3.99	<0.01	4.00	<0.01	4.97	0.01	4.99	0.01
Oxygen	4		4		6		6		8		8	
	Molecular proportions											
Fo	76		76		En	79		48	Ab	85		86
Fa	24		24		Fs	20		8	An	10		10
					Wo	1		45	Or	4		4

n = number of analyses; # = all iron is assumed as ferrous; av = average compositions of the minerals; σ = standard deviation at 1σ; and n.d. = not detected. Detection limit (in wt%): TiO_2 = 0.02, Al_2O_3 = 0.02, Cr_2O_3 = 0.03, NiO = 0.03, and CaO = 0.01 for olivine and wadsleyite, and Cr_2O_3 = 0.03, Na_2O = 0.01, and K_2O = 0.01 for enstatite and diopside.

the original olivine in contact with the matrix of the SMVs (Rw (1) in Fig. 4). These crystallites form thin ringwoodite rims of 0.1–2.5 μm width. The second occurrence is in the form of sets of ringwoodite lamellae in the original olivine (Rw (2) in Fig. 4). The width of the ringwoodite lamellae is 0.2–2.5 μm. We could not obtain the chemical composition of these two types of ringwoodite crystallites because they were too small for the measurement by EPMA. The third occurrence is represented by the polycrystalline aggregates of ringwoodite where the original olivine appears to have been completely replaced by ringwoodite (Rw (3) in Fig. 4). The width of the ringwoodite aggregates is 10–70 μm. Raman spectroscopy data imply that a small amount of wadsleyite is contained in the ringwoodite aggregates (Fig. 7c). The bulk composition of the ringwoodite aggregates (Fo_{76}) is identical to that of the original olivine (Fo_{76}) (Table 2).

Some original coarse-grained enstatite grains in the SMVs have been replaced by polycrystalline aggregates of majorite (Figs. 5 and 7d). Individual majorite crystals have a spindle-like shape with a size of 2.0 μm in length and 0.5 m in width (Fig. 5a). Polycrystalline majorite was also observed along the grain boundaries and fractures of the original coarse-grained enstatite (Figs. 5b and 5c). The grain size of the individual majorite is up to 3.0 μm and some majorite crystallites nucleated along the fractures have an elongated shape orientated perpendicular to the fractures. The chemical composition of the majorite ($En_{78}Fs_{21}Wo_2$) is almost identical to that of the original enstatite ($En_{79}Fs_{20}Wo_1$) (Table 2). In particular, there is no significant enrichment of Na, Al, and Ca concentrations in the majorite, which is generally observed in majorite-pyrope solid solutions crystallized from chondrite melts (Chen et al. 1996; Xie et al. 2001b; Ohtani et al. 2004; Xie et al. 2006; Zhang et al. 2006). Polycrystalline aggregates

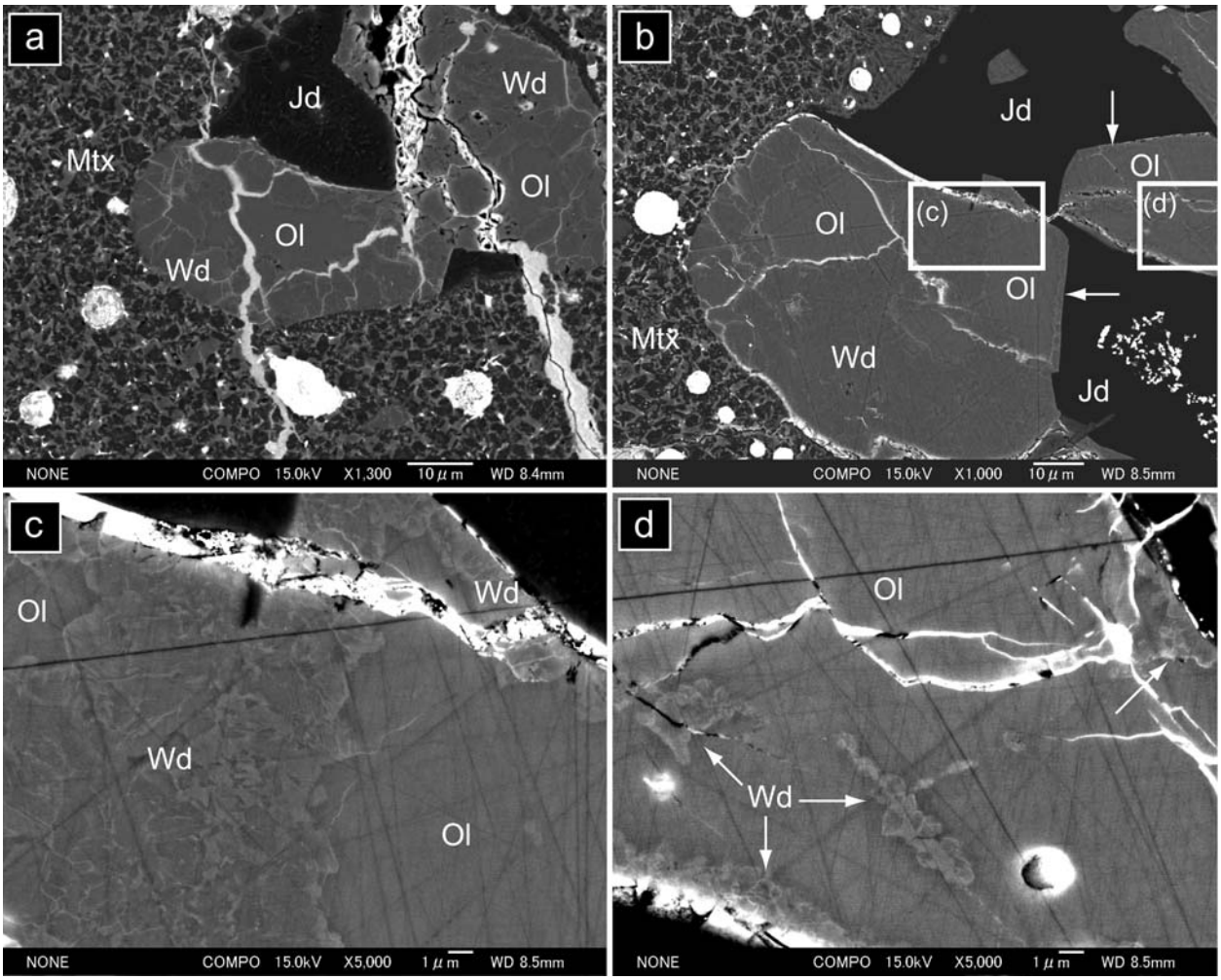

Fig. 2. BSE images of the original olivine replaced by wadsleyite in the coarse-grained fragments of host rock entrained in the SMVs of Sahara 98222. a) The wadsleyite mainly exists along the original olivine grain margins in contact with the matrix of the SMV. b) The wadsleyite also occurs along the olivine grain margins not in contact with the matrix of the SMV (white arrows). c) A magnified image of the box labeled c in (b). The wadsleyite exits as polycrystalline aggregates. d) A magnified image of the box labeled d in (b). The wadsleyite occurs along fractures of the original olivine. Ol = olivine; Wd = wadsleyite; Jd = jadeite-containing grains; and Mtx = matrix of the SMVs.

of akimotoite were also identified in the coarse-grained fragments of host rock within the SMVs, replacing the original coarse-grained enstatite (Figs. 5d and 7e). Individual akimotoite crystals are granular with a diameter up to 1.0 μm. The chemical composition of the akimotoite ($En_{78}Fs_{20}Wo_1$) is similar to that of the original enstatite ($En_{79}Fs_{20}Wo_1$) (Table 2).

Lingunite, $NaAlSi_3O_8$-hollandite, was observed in coarse-grained fragments of host rock in the SMVs or in the host rock adjacent to the SMVs (Figs. 6 and 7f). The lingunite coexists with maskelynite or jadeite-containing assemblages that are similar to the jadeite-containing grains identified from Sahara 98222. Where lingunite and the jadeite-containing assemblages coexist, the jadeite-containing assemblages have a vein-like texture with the coexisting lingunite (Fig. 6), although the crystallographic relationship has not yet been clarified. Such a texture has not been reported so far. The average chemical composition of the lingunite ($Ab_{87}An_7Or_5$) is a little different from that of maskelynite ($Ab_{83}An_{10}Or_7$) (Table 2). This difference could be due to the difference in the analytical procedure and conditions used; for example, the loss of volatile Na from the lingunite could be reduced by using the dedicated cooling stage during the EPMA measurements. The composition of the jadeite-containing assemblages ($Ab_{90}An_7Or_3$) shows a relatively higher Ab ratio and lower Or ratio compared with the coexisting lingunite ($Ab_{87}An_8Or_6$) (Table 2).

DISCUSSION

Transformation Mechanisms from Olivine to Wadsleyite

Wadsleyite has been identified in many shocked ordinary chondrites, Martian meteorites, and lunar meteorites (e.g.,

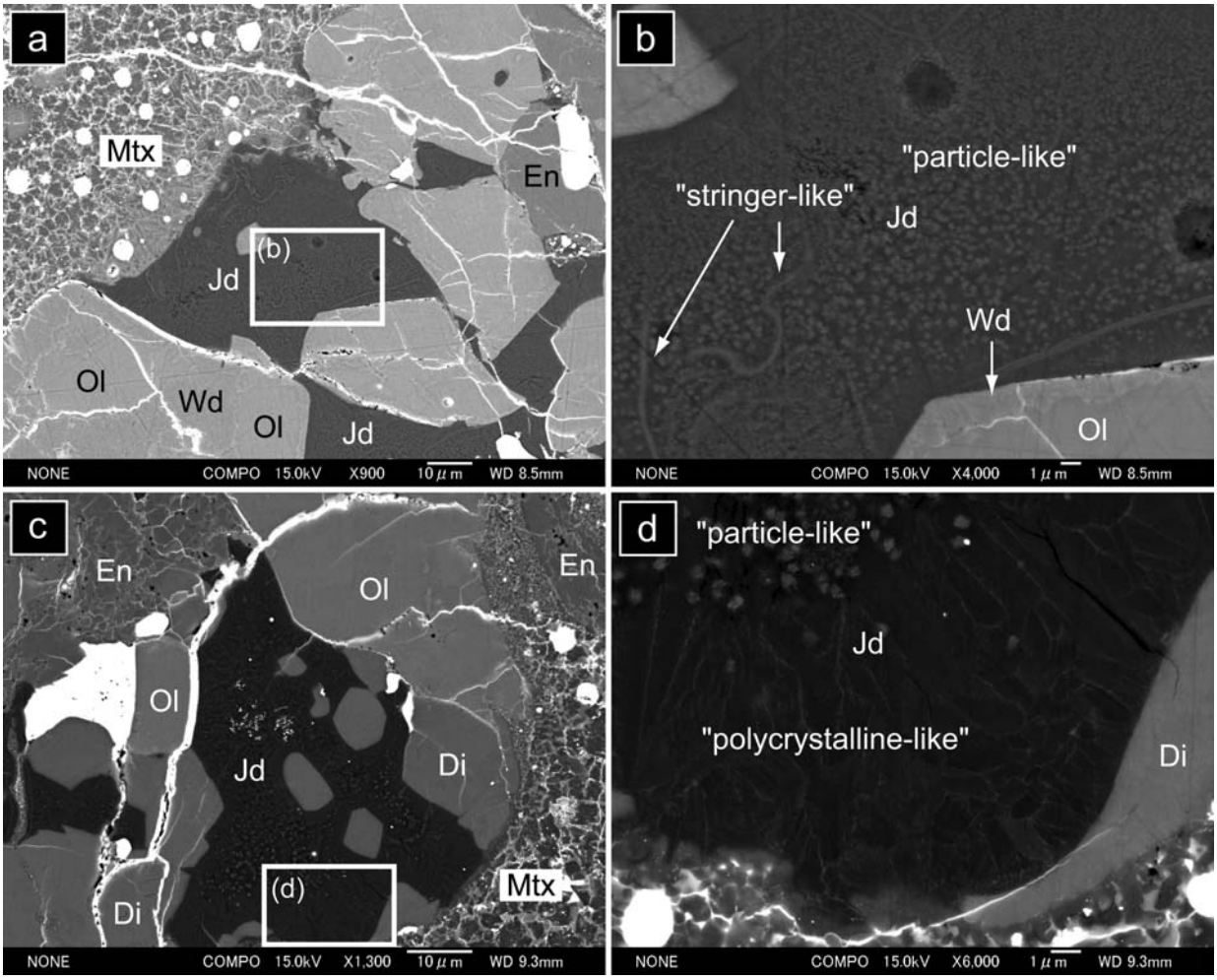

Fig. 3. BSE images of the jadeite-containing grains in Sahara 98222. a and c) The jadeite-containing grains in coarse-grained fragments of host rock entrained in the SMVs. b) A magnified image of the box in (a). Numerous "particle-like" and "stringer-like" phases were observed inside the grains. d) A magnified image of the box in (c). A "polycrystalline-like" phase was observed along the grain margins adjacent to the matrix of the SMV. Ol = olivine; Wd = wadsleyite; En = enstatite; Di = diopside; Jd = jadeite-containing grains; and Mtx = matrix of the SMVs.

Putnis and Price 1979; Madon and Poirier 1983; Price 1983; Price et al. 1983; Kimura et al. 2000; Malavergne et al. 2001; Barrat et al. 2005). Most previously reported wadsleyite has been associated with ringwoodite. Some previous studies proposed that wadsleyite was formed from ringwoodite by a back-transformation during pressure release (Putnis and Price 1979; Madon and Poirier 1983; Price 1983). The occurrence of wadsleyite with either trace or no ringwoodite is rare (Price et al. 1983; Kimura et al. 2000; Malavergne et al. 2001). Nevertheless, we found pervasive isolated wadsleyite in the original olivine grains entrained in the SMVs of Sahara 98222 (Figs. 2 and 7a). The identical chemical compositions of the olivine and wadsleyite indicate that the wadsleyite in Sahara 98222 was formed from olivine through a solid-state transformation mechanism (Table 1). If the wadsleyite had crystallized from a melt, then the chemical composition of the wadsleyite would become different from that of the original olivine. Miyahara et al. (2008) reported that chemically different wadsleyite ($Fa_{6–10}$) and ringwoodite ($Fa_{28–38}$) coexist in the same grains that were originally homogeneous olivine ($Fa_{24–26}$). They proposed that the melting of the original olivine is followed by a fractional crystallization of Mg-rich wadsleyite and Fe-rich ringwoodite under high-pressure conditions. On the other hand, in the case of our wadsleyite (Fa_{24}), it has the same chemical composition as that of the original olivine (Fa_{24}) (Table 1). This observation was also reported from experiments on olivine-wadsleyite transformation kinetics (e.g., Kubo et al. 1998; Mosenfelder et al. 2000). Therefore, it is considered that the wadsleyite we observed was formed by a solid-state phase transformation from the original olivine.

High-pressure and high-temperature experiments on the kinetics of the olivine-wadsleyite phase transition have been conducted in the stability field of wadsleyite (13.4–17 GPa and 850–1100 °C) using a multi-anvil apparatus (Brearley et al. 1992; Kubo et al. 1998, 2004; Mosenfelder et al. 2000). Brearley et al. (1992) and Kubo et al. (2004) used olivine powder as the starting material and the grain size of the

olivine crystals before the reaction was 2–18 μm. In their recovered samples, they identified that wadsleyite nucleated along grain boundaries or at triple junctions of olivine grains. On the other hand, Kubo et al. (1998) and Mosenfelder et al. (2000) used olivine single crystals as their starting material with grain sizes of 500–1000 μm. They also reported nucleation of wadsleyite on the surface of the olivine single crystals forming wadsleyite rims that grew inwards from the rims with time. The wadsleyite crystallites had an elongated shape oriented perpendicular to the surface of the olivine single crystals, and there was no topotaxial relationship between the olivine and the wadsleyite. In our sample, the wadsleyite occurs along the grain boundaries or fractures of olivine, and there seems to be no crystallographic relationship between olivine and wadsleyite (Fig. 2). Some large wadsleyite crystals along the grain boundaries near SMVs have a columnar shape elongated perpendicular to the grain boundaries of the original olivine (Figs. 2a and 2b). The textural characteristics of experimentally formed wadsleyite and natural wadsleyite are in good agreement with each other. Kubo et al. (1998) and Mosenfelder et al. (2000) also reported that there was no difference in the chemical composition and the Fe/Mg ratio between olivine and wadsleyite. This is also consistent with our results, where the chemical composition of the wadsleyite in Sahara 98222 is identical to that of the original olivine (Table 1). Therefore, the wadsleyite in the SMVs of Sahara 98222 provides natural evidence supporting the suggestion based on experimental works that the mechanism of the olivine-wadsleyite phase transformation is incoherent grain boundary nucleation and an interface-controlled growth mechanism (Brearley et al. 1992; Kubo et al. 1998, 2004; Mosenfelder et al. 2000).

Transformation Mechanisms from Olivine to Ringwoodite

We observed three different occurrences of ringwoodite in the SMVs of Yamato 74445 (Fig. 4). The identical chemical compositions of ringwoodite and the original olivine suggest that the ringwoodite was formed from the original olivine by a solid-state transformation. High-pressure and high–temperature experiments on the kinetics of the olivine-ringwoodite phase transition have proposed two different mechanisms: grain boundary nucleation and intracrystalline lamellae nucleation (Rubie and Ross 1994; Kerschhofer et al. 1996, 2000; Mosenfelder et al. 2001). The mechanism of grain boundary nucleation in the olivine-ringwoodite transformation is well documented in the papers of Kerschhofer et al. (1996, 2000) and Mosenfelder et al. (2001). Nucleation of ringwoodite or wadsleyite occurs most easily on the grain boundaries of original olivine because of the high energy of these defects compared with intracrystalline defects such as dislocations and subgrain boundaries. When the nucleation rate is high, the grain boundaries become rapidly saturated with the new phases. The olivine grains are then separated by continuous rims of the product phases and are gradually consumed by the growth of these rims. In the case of the olivine-ringwoodite transformation in shock melt veins, there is another important parameter—the thermal gradient within the original olivine grains. The grain boundaries of the olivine in contact with the matrix of the shock melt veins are hotter than the grain interiors, so that the phase transformation would be promoted more at the grain boundaries. We identified that ringwoodite crystallites nucleated along the grain margins of the original olivine (Rw (1) in Fig. 4), and this would be the result of the grain boundary nucleation mechanism. We also identified a ringwoodite texture formed from another mechanism, i.e., the intracrystalline lamellae nucleation mechanism, as shown by Rw (2) in Fig. 4. Our observations of ringwoodite lamellae in the original olivine are similar to those reported by Ohtani et al. (2004) and Chen et al. (2004). The polycrystalline aggregates of ringwoodite (Rw (3) in Fig. 4), where the olivine-ringwoodite transformation seems to be complete, could have formed by either the grain boundary mechanism, or the intracrystalline mechanism, or a combination of both mechanisms.

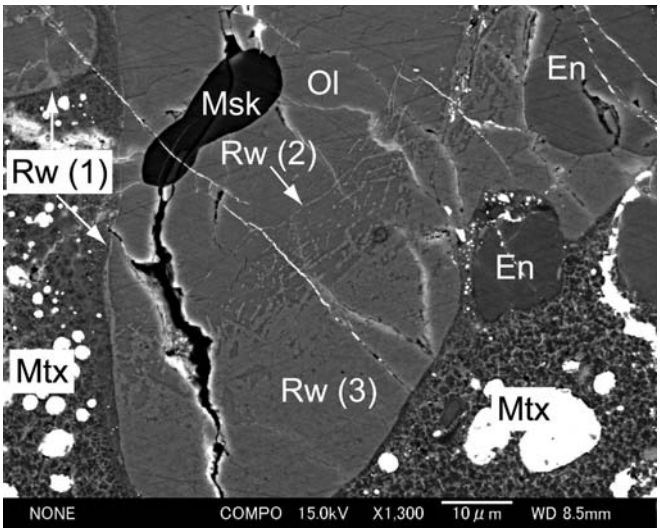

Fig. 4. A BSE image of the original olivine replaced by ringwoodite in the host rock adjacent to a SMV in Yamato 74445. Three different occurrences of ringwoodite were identified: (1) ringwoodite crystallites along the grain margins of the original olivine, (2) sets of ringwoodite lamellae, and (3) polycrystalline aggregates of ringwoodite. Ol = olivine; Rw = ringwoodite; En = enstatite; Msk = maskelynite; and Mtx = matrix of the SMV.

Transformation Mechanisms from Enstatite to Majorite

Previous studies reported that some majorite was crystallized from chondrite melts under high-pressure and high–temperature conditions (e.g., Smith and Mason 1970; Chen et al. 1996; Xie et al. 2001b; Ohtani et al. 2004; Xie et al. 2006; Zhang et al. 2006). This type of majorite shows a significant enrichment in Al, Ca, and Na concentrations compared with the composition of enstatite in host rocks, and

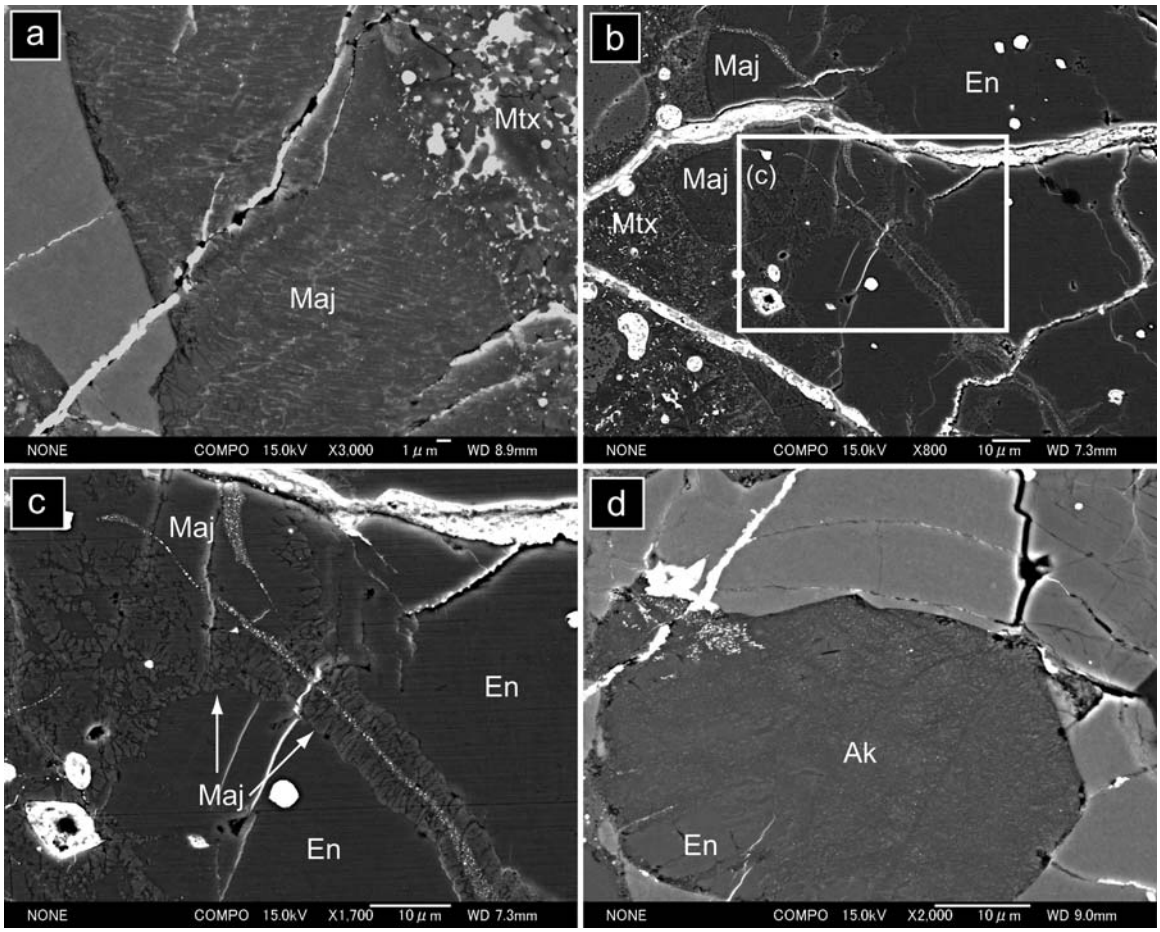

Fig. 5. BSE images of the original enstatite replaced by majorite and akimotoite in SMVs of Yamato 74445. a) Aggregates of spindle-like majorite replacing the original enstatite in a coarse-grained fragment of host rock entrained in the SMV. b) Polycrystalline aggregates of majorite along grain margins of the original enstatite adjacent to the matrix of the SMV. c) A magnified image of the box in (b). Majorite also nucleated along the fractures of the original enstatite. d) Akimotoite replacing the original enstatite in a coarse-grained fragment of host rock within the SMV. En = enstatite; Maj = majorite; Ak = akimotoite; and Mtx = matrix of the SMVs.

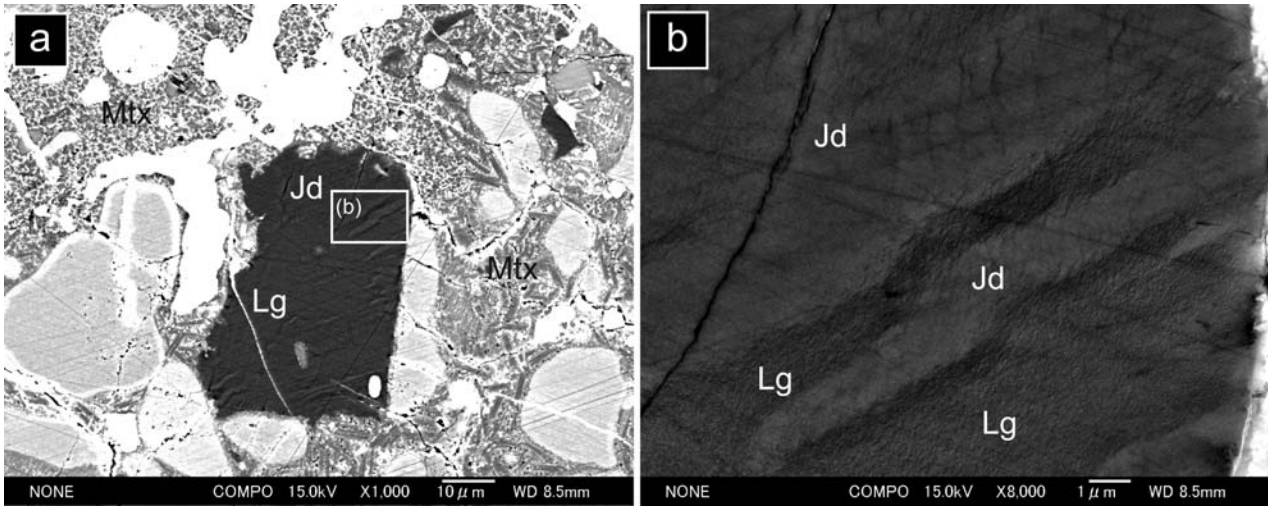

Fig. 6. BSE images of the original plagioclase replaced by lingunite ($NaAlSi_3O_8$-hollandite) and jadeite-containing assemblages in a coarse-grained fragment of host rock entrained in the SMV of Yamato 74445. a) Coexistence of lingunite and jadeite. b) A magnified image of the box in (a). The jadeite-containing assemblage shows a vein-like texture. Lg = lingunite; Jd = jadeite-containing assemblage; and Mtx = matrix of the SMV.

forms a majorite-pyrope solid solution. This majorite-pyrope solid solution comprises the matrix of the SMVs and it has an idiomorphic granular texture. Another type of majorite has also been reported, which was formed by a solid-state transformation from the original enstatite within coarse-grained fragments of host rock in SMVs (Chen et al. 1996; Xie et al. 2001b; Ohtani et al. 2004; Zhang et al. 2006; Xie and Sharp 2007). This majorite has an identical chemical composition to that of the original enstatite.

We observed polycrystalline aggregates of spindle-like majorite in the coarse-grained fragments of host rock entrained in the SMVs of Yamato 74445 (Fig. 5a) and majorite crystallites along the grain margins and fractures of the original enstatite (Figs. 5b and 5c). The observed spindle-like or elongated morphology of the individual majorite crystallites is different from the idiomorphic morphology of the majorite-pyrope solid solution crystallized from a chondrite melt. The chemical composition of our majorite is almost identical to that of the original enstatite (Table 2), without any significant enrichment of Na, Al, and Ca that generally occurs in majorite-pyrope solid solutions crystallized from chondrite melts. This suggests that our majorite was formed from the original enstatite by a solid-state transformation mechanism under shock loading. Unfortunately, neither the kinetics nor the mechanism of the polymorphic enstatite-majorite phase transformation has been determined experimentally. Our observations on natural majorite suggest that the nucleation and growth of majorite along grain boundaries or fractures is a possible mechanism for the enstatite-majorite phase transformation.

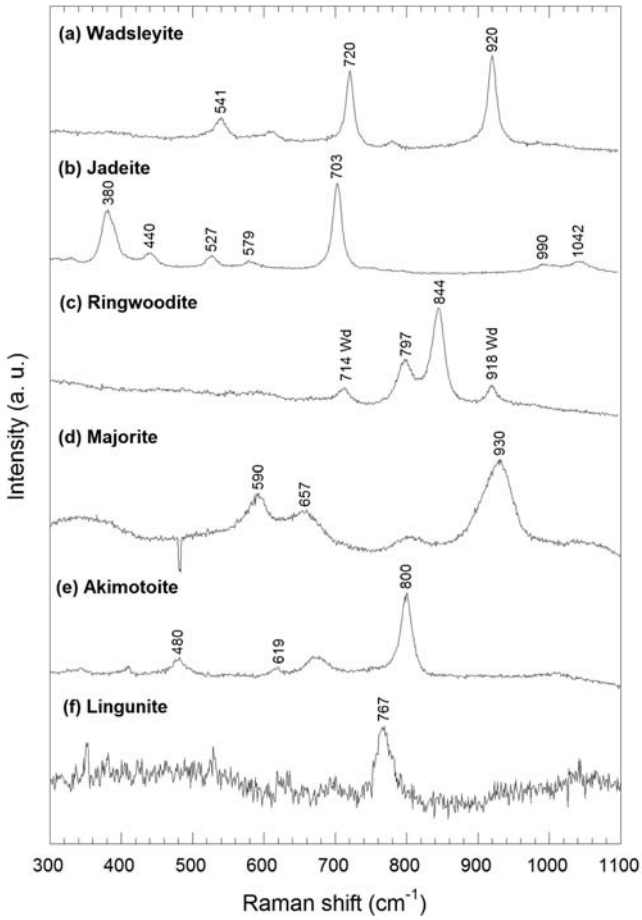

Fig. 7. Raman spectra of high-pressure minerals identified in the SMVs of Sahara 98222 and Yamato 74445 L6 chondrites. Wd = wadsleyite.

Transformation Mechanisms from Enstatite to Akimotoite

We identified polycrystalline aggregates of akimotoite in the coarse-grained fragments of host rock entrained in the SMVs of Yamato 74445 (Fig. 5d). These aggregates have an identical chemical composition to that of the original enstatite, indicating that the akimotoite was formed from the original enstatite by a solid-state transformation mechanism. Akimotoite formed from enstatite by a solid-state transformation mechanism has been reported in SMVs from some shocked chondrites (Tomioka and Fujino 1997, 1999; Ohtani et al. 2004; Zhang et al. 2006; Ferroir et al. 2008). Tomioka and Fujino (1997) reported two different morphologies of akimotoite coexisting with clinoenstatite. One is granular-shaped, and the other is columnar-shaped. The former akimotoite has no crystallographic relationship with the adjacent clinoenstatite, whereas the latter akimotoite (Ak) exhibits a topotaxial relationship with clinoenstatite (Cen) of $(100)_{Cen}$ // $(0001)_{Ak}$, $(010)_{Cen}$ // $(10–10)_{Ak}$. To explain the genesis of the columnar-shaped akimotoite with a topotaxial relationship to clinoenstatite, Tomioka (2007) proposed a shear mechanism model for the enstatite-akimotoite phase transformation. Recently, Ferroir et al. (2008) reported two different occurrences of akimotoite: polycrystalline aggregates and sets of lamellae. The akimotoite in Yamato 74445 occurs as polycrystalline aggregates of granular crystals, and there appears to be no topotaxial relationship between the original enstatite and the individual akimotoite crystals. The features of our akimotoite are similar to those of the granular-shaped akimotoite (Tomioka and Fujino 1997) and/or the polycrystalline aggregates of akimotoite (Ferroir et al. 2008). The absence of a crystallographic relationship between the original enstatite and the akimotoite indicates that the akimotoite in Yamato 74445 was formed by a different mechanism from the shear model proposed by Tomioka (2007). It is considered that the polycrystalline aggregates of akimotoite were formed by an incoherent nucleation and growth mechanism.

Jadeite-Containing Assemblages with Albitic Composition

High-pressure and high–temperature experiments indicate that albite transforms to several high-pressure mineral assemblages with increasing pressure, following the

Table 2. Chemical compositions of the minerals and glass in the Yamato 74445 L6 chondrite obtained using EPMA-WDS.

	Olivine		Ringwoodite		Enstatite		Diopside		Majorite		Akimotoite		Maskelynite		Lingunite		Jadeite
n	10		11		5		10		3		9		7		3		1
	Chemical composition (wt%)																
	av	σ	av	σ	av	σ	av	σ	av	σ	av	σ	av	σ	av	σ	
SiO_2	38.43	0.32	38.65	0.26	56.09	0.14	54.11	0.24	55.84	0.23	56.12	0.33	65.79	0.52	67.25	0.39	67.30
TiO_2	n.d.	–	n.d.	–	0.16	0.01	0.44	0.04	0.20	0.05	0.18	0.03	–	–	–	–	–
Al_2O_3	n.d.	–	n.d.	–	0.16	0.02	0.47	0.03	0.15	0.02	0.14	0.03	21.24	0.24	21.56	0.20	21.43
Cr_2O_3	n.d.	–	n.d.	–	0.12	0.02	0.85	0.06	n.d.	–	n.d.	–	–	–	–	–	–
FeO#	21.75	0.53	21.64	0.35	13.04	0.16	4.86	0.22	13.70	0.66	13.33	0.32	0.32	0.08	0.54	0.10	0.42
MnO	0.43	0.04	0.42	0.03	0.42	0.03	0.22	0.02	0.47	0.06	0.46	0.02	–	–	–	–	–
NiO	n.d.	–	n.d.	–	–	–	–	–	–	–	–	–	–	–	–	–	–
MgO	39.12	0.42	39.11	0.46	29.33	0.10	16.70	0.16	28.99	0.73	29.06	0.40	–	–	–	–	–
CaO	n.d.	–	n.d.	–	0.68	0.19	21.44	0.21	0.97	0.49	0.69	0.32	2.02	0.13	1.38	0.02	1.37
Na_2O	–	–	–	–	n.d.	–	0.57	0.04	n.d.	–	n.d.	–	9.37	0.18	8.92	0.42	9.20
K_2O	–	–	–	–	n.d.	–	n.d.	–	n.d.	–	n.d.	–	1.24	0.19	0.85	0.12	0.44
Total	99.74	0.39	99.82	0.49	100.00	0.17	99.64	0.34	100.32	0.29	99.97	0.46	99.97	0.38	100.50	0.26	100.15
	Cation formula																
Si	1.00	<0.01	1.00	<0.01	2.00	<0.01	1.99	<0.01	1.99	<0.01	2.00	<0.01	2.90	0.01	2.93	0.01	2.93
Ti	–	–	–	–	<0.01	<0.01	0.01	<0.01	0.01	<0.01	<0.01	<0.01	–	–	–	–	–
Al	–	–	–	–	0.01	<0.01	0.02	<0.01	0.01	<0.01	0.01	<0.01	1.10	0.01	1.11	0.01	1.10
Cr	–	–	–	–	<0.01	<0.01	0.02	<0.01	–	–	–	–	–	–	–	–	–
Fe#	0.47	0.01	0.47	0.01	0.39	<0.01	0.15	0.01	0.41	0.02	0.40	0.01	0.01	<0.01	0.02	<0.01	0.02
Mn	0.01	<0.01	0.01	<0.01	0.01	<0.01	0.01	<0.01	0.01	<0.01	0.01	<0.01	–	–	–	–	–
Ni	–	–	–		–	–	–	–	–	–	–	–	–	–	–	–	–
Mg	1.52	0.01	1.51	0.01	1.56	<0.01	0.91	0.01	1.54	0.04	1.54	0.02	–	–	–	–	–
Ca	–	–	–	–	0.03	0.01	0.84	0.01	0.04	0.02	0.03	0.01	0.10	0.01	0.06	<0.01	0.06
Na	–	–	–	–	–	–	0.04	<0.01	–	–	–	–	0.80	0.02	0.75	0.04	0.78
K	–	–	–	–	–	–	–	–	–	–	–	–	0.07	0.01	0.05	0.01	0.02
Total	3.00	<0.01	3.00	<0.01	3.99	<0.01	4.00	<0.01	4.00	<0.01	3.99	<0.01	4.98	0.01	4.92	0.03	4.92
Oxygen	4		4		6		6		6		6		8		8		8
	Molecular proportions																
Fo	76		76		En	79	48		78		78		Ab	83	87		90
Fa	24		24		Fs	20	8		21		20		An	10	7		7
					Wo	1	44		2		1		Or	1	5		3

n = number of analyses; # = all of iron is assumed as ferrous; av = average compositions of the minerals; σ = standard deviation at 1σ; and n.d. = not detected.
Detection limit is the same as listed in the caption of Table 1.

sequence: albite → jadeite + quartz (coesite, stishovite) → $NaAlSi_3O_8$-hollandite (lingunite) or calcium ferrite-type $NaAlSiO_4$ + stishovite (Liu 1978; Yagi et al. 1994; Tutti 2007). The jadeite found in Sahara 98222 could have formed by decomposition of the original albitic plagioclase under high-pressure and high–temperature conditions during the shock event. However, Raman spectroscopy did not detect any evidence for crystalline silica phases, which should accompany jadeite after decomposition of plagioclase (Fig. 7b). Such an occurrence of jadeite in extraterrestrial samples was already reported by Kimura et al. (2000), and was also described in some L6 chondrites (Ohtani et al. 2004).

Kubo et al. (2008) studied the crystallization kinetics of jadeite and silica phases from albite under high-pressure and high–temperature conditions using a multi-anvil apparatus. They compressed natural albite ($Ab_{98.0}An_{0.4}Or_{1.6}$) to set pressures, and then increased the temperature. As the temperature increased, albite vitrified and then jadeite nucleated from the amorphous albite. The nucleation of silica phases, such as stishovite, occurred significantly later than the nucleation of jadeite. This result suggests that the natural occurrence of jadeite without any crystalline silica phases would be produced by short duration high-pressure and high–temperature conditions during an impact event. Based on the results and calculations of Kubo et al. (2008), when the albite experiences the static conditions of 1200–1700 °C and 20 GPa lasting for 1 second, only jadeite would form. Both jadeite and stishovite would crystallize at higher temperatures than 1700 °C, whereas both jadeite and stishovite would not form at lower temperatures than 1200 °C. If the duration of the static high-pressure and high-temperature conditions is 10 seconds, the kinetic boundaries between the temperature ranges for the formation of jadeite + stishovite, only jadeite, and neither of them would shift to lower temperatures by 200–400 °C. Although we do not know the exact temperature conditions which the jadeite-containing grains experienced during the shock event, it could have been slightly lower than the temperature of the SMVs (>1900 °C for Sahara 98222), which will be discussed later in the following paragraph. If the temperature of the jadeite-containing grains is assumed to be 1700–1800 °C, then this is close to the upper bound of the temperature range for the formation of only jadeite (1200–1700 °C) on the duration of 1 second. If the temperature of the jadeite-containing grains was higher, then the duration of the high-pressure and high-temperature conditions during the shock event should have been less than 1 second for the formation of only jadeite, without any crystalline silica phases. Thus, the duration of the high-pressure and high-temperature state during the impact event in Sahara 98222 would be ~1 second. This would be consistent with previously reported shock duration times for other L6 chondrites (0.04–4 seconds) estimated using different approaches (Ohtani et al. 2004; Beck et al. 2005; Xie et al. 2006).

Regarding the complicated texture of the jadeite-containing grains, James (1969) reported a similar occurrence of jadeite-containing grains in impact metamorphosed amphibolite from the Ries impact crater, Germany. James identified jadeite using X-ray diffraction techniques on maskelynite with an oligoclase composition, but did not detect any evidence of crystalline silica phases. Optical and electron microscopic images showed that the maskelynite contains some particles with a relatively high refractive index, and most of these were distributed in irregular stringers. Based on the measurements and calculations of their refractive indices, James concluded that the particles are mixtures of jadeite and an amorphous phase that had a composition of oligoclase minus jadeite. The occurrence of particles and stringers in the jadeite-containing maskelynite from the Rise crater is similar to our observations of the jadeite-containing grains in the SMVs of Sahara 98222 (Fig. 3). The observed "particle-like" and "stringer-like" phases in Sahara 98222 could also be composed of jadeite + an amorphous phase.

In addition, we observed that the intensity of the Raman peak from jadeite (around 700 cm^{-1}) was stronger at the grain margins near the SMVs than in the interior of the grains. This suggests that the amount of jadeite crystallites and/or their degree of crystallinity at the grain margins (dominated by the "polycrystalline-like" phase) is greater than that in the grain interiors (dominated by the "particle-like" or "stringer-like" phases). In other words, the nucleation and growth of jadeite would be promoted with increasing temperature, and the texture of the jadeite-containing assemblage would change from the "particle-like" and "stringer-like" phases to the "polycrystalline-like" phase with progressive nucleation and growth of jadeite.

Coexistence of Lingunite and Jadeite-Containing Assemblages

Lingunite, $NaAlSi_3O_8$-hollandite, was first identified in the SMVs of the Tenham L6 chondrite, and then in many shocked chondrites or Martian meteorites (El Goresy et al. 2000; Gillet et al. 2000; Kimura et al. 2000; Tomioka et al. 2000; Ohtani et al. 2004; Xie et al. 2004, 2007). Tomioka et al. (2000) proposed that lingunite was formed from the host plagioclase by a solid-state transformation. On the other hand, Gillet et al. (2000) proposed that lingunite was crystallized from a feldspathic melt. In Yamato 74445, we identified lingunite coexisting with maskelynite or jadeite-containing assemblages in the coarse-grained fragments of host rock within the SMVs, or in the host rocks adjacent to the SMVs (Figs. 6 and 7f). The coexistence of lingunite and jadeite has also been reported in previous studies (El Goresy et al. 2000; Gillet et al. 2000; Kimura et al. 2000). In our coexisting lingunite and jadeite-containing assemblages, there appears to be a possible crystallographic relationship between the

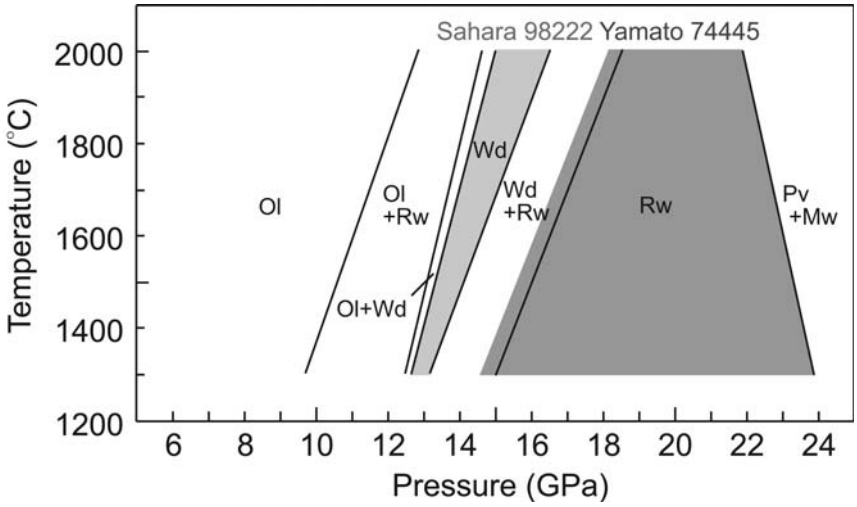

Fig. 8. Pressure-temperature phase diagram of olivine (Fo_{76}) (after Ito and Takahashi 1989; Katsura and Ito 1989). The two hatched regions correspond to the estimated shock pressure conditions for Sahara 98222 and Yamato 74445, respectively. Ol = olivine; Wd = wadsleyite; Rw = ringwoodite; Pv = (Mg, Fe)SiO_3-perovskite; and Mw = magnesiowüstite.

jadeite-containing assemblages and the lingunite, although the details of the crystallographic relationship have not yet been determined. This possible crystallographic relationship is likely the result of a solid-state transformation from the original crystalline plagioclase or an amorphous phase that maintained some crystallographic features of the original crystalline plagioclase. The chemical composition of the jadeite-containing assemblage ($Ab_{90}An_7Or_3$) shows a relatively higher Ab component and a lower Or component compared with the coexisting lingunite ($Ab_{87}An_8Or_6$). This difference may originate from the diffusion of Na into jadeite and K into lingunite during the transformation, although the diffusion rates have not yet been measured.

Pressure and Temperature Conditions During the Shock Events

Based on the constituent mineral assemblages in the SMVs and their pressure-temperature stability fields determined from static high-pressure experiments, we estimated the pressure conditions of the shocked chondrites during the impact events. Figure 8 shows a phase diagram of olivine with the composition of Fo_{76}, which is the average composition of olivine in our chondrites (after Ito and Takahashi 1989; Katsura and Ito 1989). Figure 9 shows a phase diagram of the enstatite–ferrosilite join at 1800 C (after Ohtani et al. 1991). The vertical dotted line in Fig. 9 corresponds to the average composition of enstatite (En_{79}) in our chondrites. In the case of Sahara 98222, it contains abundant wadsleyite, but we could not identify ringwoodite (Figs. 2 and 7a). Thus, Sahara 98222 would have experienced pressure conditions within the stability field of wadsleyite, 13–16 GPa (Fig. 8). We did not find any high-pressure polymorphs of enstatite in Sahara 98222. This result would constrain the pressure conditions of Sahara 98222 to below the pyroxene-majorite phase boundary, that is <16 GPa (Fig. 9). The plagioclase in the SMVs of Sahara 98222 has been replaced by jadeite (Figs. 3 and 7b). However, it has not been transformed into lingunite or calcium ferrite-type $NaAlSiO_4$ + stishovite. This indicates that the shock pressure corresponded to the stability field of jadeite, ranging from 2.5 to 22 GPa (Liu 1978; Yagi et al. 1994; Tutti 2007). Based on these considerations, we estimated the shock pressure conditions of Sahara 98222 to be 13-16 GPa. Yamato 74445 contains abundant ringwoodite accompanied by a slight amount of wadsleyite, and we did not find any silicate perovskite (Figs. 4 and 7c). Thus, the shock pressure conditions of Yamato 74445 would have been from the uppermost stability field of wadsleyite + ringwoodite to the stability field of ringwoodite, 14–24 GPa (Fig. 8). Yamato 74445 also contains both majorite and akimotoite (Figs. 5, 7d, and 7e), indicating that the pressure conditions would have been in the range of their stability fields, 17–24 GPa (Fig. 9). We identified lingunite and some coexisting jadeite-containing assemblages (Figs. 6 and 7f). This implies that the shock pressure would have been from the uppermost stability field of jadeite to the stability field of lingunite, i.e., from 17 to 24 GPa (Liu 1978; Yagi et al. 1994; Tutti 2007). Based on these considerations, we constrained the shock pressure of Yamato 74445 to 17–24 GPa.

The shock pressure of Yamato 74445 estimated from the high-pressure mineral assemblages in the SMVs (17–24 GPa) appears to be similar to other L6 chondrites previously reported, e.g., 18–23 GPa for Yamato 791384, ~23 GPa for Sixiangkou, ~23 GPa for Suizhou, and ~ 25 GPa for Tenham (Chen et al. 2004; Ohtani et al. 2004; Xie and Sharp 2004; Beck et al. 2005; Xie et al. 2006). On the other hand, the shock pressure of Sahara 98222 (13–16 GPa) is relatively

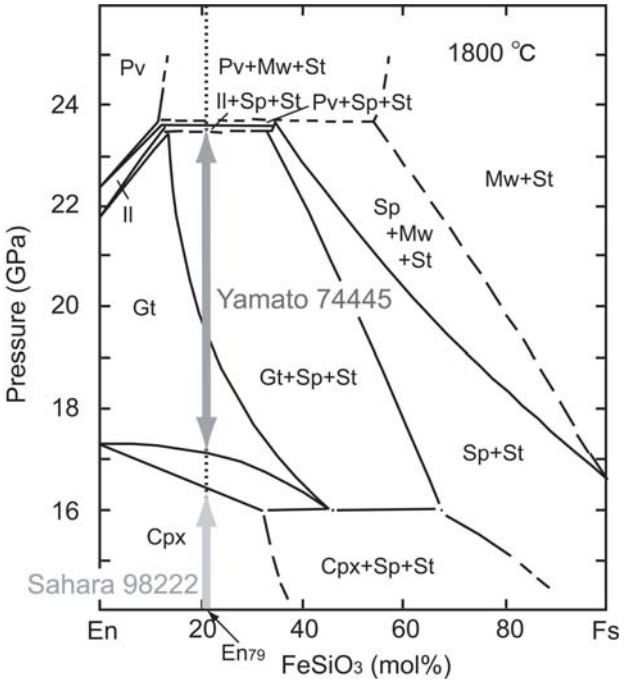

Fig. 9. Phase diagram of the enstatite-ferrosilite join at 1800 °C (after Ohtani et al. 1991). The vertical dotted line represents the average chemical composition of enstatite (En_{79}) in Sahara 98222 and Yamato 74445. The two arrows show possible pressure conditions achieved during the shock events in each chondrite. Cpx = Ca-poor clinopyroxene; Gt = $(Mg,Fe)SiO_3$-garnet (majorite); Il = $(Mg,Fe)SiO_3$-ilmenite (akimotoite); Pv = $(Mg,Fe)SiO_3$-perovskite; Sp = $(Mg,Fe)_2SiO_4$-spinel (ringwoodite); St = stishovite; and Mw = magnesiowüstite.

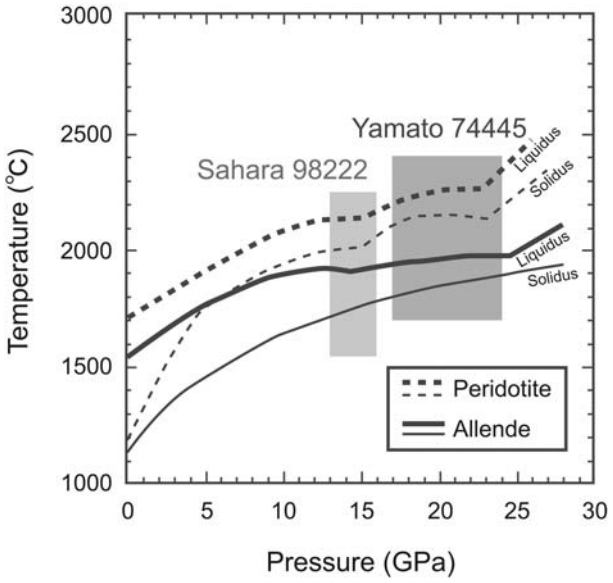

Fig. 10. The melting relationship of the Allende CV chondrite (solid lines) and KLB1 peridotite (dashed lines) (after Zhang end Herzberg 1994; Agee et al. 1995; Asahara et al. 2004). The two hatched regions correspond to the estimated pressure ranges of Sahara 98222 (13–16 GPa) and Yamato 74445 (17–24 GPa).

lower than that of other L6 chondrites. It has been reported that the shock pressure is proportional to impact velocity during the collision (Melosh 1989). The difference in shock pressures suggests that Sahara 98222 could have experienced a collision with an impact velocity that was relatively slower than that of the other L6 chondrites. Alternatively, the parent rock of Sahara 98222 could have existed in a more distant part from the center of the collision, where shock pressure induced by a planetary collision would be attenuated. However, if the previous finding of ringwoodite in Sahara 98222 is taken into account, then the estimated pressure will shift to a higher value, which would be consistent with the shock pressure for Yamato 74445 and other L6 chondrites. In this case, there could have been pressure or temperature heterogeneity within the parent rock of Sahara 98222.

It is possible to estimate the temperature conditions of the SMVs in these chondrites. They have pervasive SMVs, and many high-pressure polymorphs are contained in the SMVs. Thus, the temperature conditions of the SMVs would have been at least above the solidus temperature under the high-pressure conditions during the shock events. We can use the results of melting experiments of a carbonaceous chondrite and a terrestrial peridotite as analogous materials of L chondrites because of the similarity in the bulk chemical compositions and constituent minerals. Figure 10 shows the results of high-pressure melting experiments on the Allende CV chondrite and KLB1 peridotite (after Zhang end Herzberg 1994; Agee et al. 1995; Asahara et al. 2004). The hatched regions correspond to the estimated pressure ranges for Sahara 98222 and Yamato 74445, respectively. L chondrites have an intermediate FeO content (14 wt% FeO) between the Allende CV chondrite (27 wt% FeO) and the KLB1 peridotite (9 wt% FeO), and it is relatively closer to that of the peridotite (Xie et al. 2006). Therefore, the solidus and liquidus temperatures of the L chondrite could also be between those of the Allende CV chondrite and the KLB1 peridotite and closer to that of the peridotite. Therefore, the temperature conditions of the SMVs in our chondrites were estimated to be >1900 °C at 13–16 GPa for Sahara 98222, and >2000 °C at 17–24 GPa for Yamato 74445.

Finally, it should be noted that the documented effects of shock processes, particularly the high-pressure phase transformations, have not progressed to completion, because of the very short duration of the impact processes. The shock pressure and temperature conditions estimated here should be qualified as "effective pressures and temperatures" during the impact events. To evaluate the impact conditions, such as pressure, temperature, and duration more accurately, further kinetic experiments with time-resolved measurements under various pressure-temperature-time conditions are needed.

CONCLUSIONS

We investigated the textures involving the high-pressure minerals in the shock melt veins of two L6 chondrites (Sahara 98222 and Yamato 74445), and related the textural

observations to the relevant transformation processes. Several high-pressure minerals were identified in coarse-grained fragments of host rock entrained in the SMVs or host rocks adjacent to the SMVs: wadsleyite and jadeite from Sahara 98222 and ringwoodite, wadsleyite, majorite, akimotoite, jadeite, and lingunite ($NaAlSi_3O_8$-hollandite) from Yamato 74445.

1. The occurrence of wadsleyite and ringwoodite along the grain boundaries of the original olivine and intracrystalline ringwoodite lamellae in the original olivine is consistent with the grain boundary and intracrystalline phase transformation mechanisms proposed by high-pressure experiments on the kinetics of olivine.
2. We reported evidence of a solid-state transformation from enstatite to majorite along the grain boundaries or fractures of the original enstatite. Polycrystalline aggregates of majorite and akimotoite were also identified. These observations suggest that an incoherent nucleation and growth mechanism could be a possible mechanism of the enstatite-majorite and enstatite–akimotoite phase transformations.
3. Jadeite-containing grains in Sahara 98222 show complicated textures with "particle-like," "stringer-like," and "polycrystalline-like" phases, and there is no evidence of crystalline silica phases. We suggest that these grains consist of jadeite crystallites plus an amorphous phase and that the chemical composition of the amorphous phase is "[original plagioclase]-[crystallized jadeite]." This assemblage would be produced by a delay in the nucleation of the silica minerals due to the short duration of the shock event.
4. We also identified the coexistence of lingunite and jadeite-containing assemblages. The jadeite-containing assemblages have a vein-like texture with a possible crystallographic relationship with the coexisting lingunite. This could suggest that it was formed by a solid-state transformation from the original plagioclase or amorphous plagioclase that maintained some crystallographic features of the original plagioclase.
5. Based on the mineral assemblages and static high-pressure experimental results, we estimated the shock pressure and temperature conditions in the SMVs of these meteorites as follows: 13–16 GPa and >1900 °C for Sahara 98222 and 17–24 GPa and >2100 °C for Yamato 74445. The lower estimated pressure for Sahara 98222 suggests that it could have experienced a collision with lower impact velocity than that of the other L6 chondrites, or its parent rock had existed in a more distant part from the center of the collision within its parent body.

Acknowledgments–We thank Prof. T. Kondo of Osaka University, Dr. H. Terasaki of Tohoku University, and Prof. A. El Goresy of Bayerisches Geoinsitutut, Universität Bayreuth, for helpful discussions and encouragements. We also thank Mr. H. Kawanobe and Mr. M. Abe for technical support in preparing the thin sections and carrying out the EPMA analyses. We would like to thank Profs. A. J. T. Jull and U. Reimold for the editorial handling, and reviewers Dr. A. Greshake and Prof. P. Buchanan for their useful comments that led to significant improvements in the paper. This work was supported by a Grant-in-aid of the Ministry of Education, Science, Sport, and Culture of Japanese government, no. 18654091 to E. O. and no. 19540500 for M. K. This work was conducted as a part of the Global Center-of-Excellence program. The first author is supported by the JSPS Research Fellowships for Young Scientists. The Yamato 74445 sample studied here was provided by the National Institute of Polar Research, Japan.

Editorial Handling—Dr. Uwe Reimold

REFERENCES

Agee C. B., Li J., Shanon M. C., and Circone S. 1995. Pressure-temperature phase diagram for the Allende meteorite. *Journal of Geophysical Research* 100:17,725–17,740.

Asahara Y., Kubo T., and Kondo T. 2004. Phase relations of a carbonaceous chondrite at lower mantle conditions. *Physics of the Earth and Planetary Interiors* 143–144:421–432.

Barrat J. A., Chaussidon M., Bohn M., Gillet P., Göpel C., and Lesourd M. 2005. Lithium behavior during cooling of a dry basalt: An ion-microprobe study of the lunar meteorite Northwest Africa 479 (NWA 479). *Geochimica et Cosmochimica Acta* 69:5597–5609.

Beck P., Gillet P., El Goresy A., and Mostefaoui S. 2005. Time scales of shock processes in chondritic and Martian meteorites. *Nature* 435:1071–1074.

Brearley A. J., Rubie D. C., and Ito E. 1992. Mechanisms of the transformations between the α, β and γ polymorphs of Mg_2SiO_4 at 15 GPa. *Physics and Chemistry of Minerals* 18:343–358.

Chen M., Sharp T. G., El Goresy A., Wopenka B., and Xie X. 1996. The majorite-pyrope + magnesiowüstite assemblage: Constraints on the history of shock veins in chondrites. *Science* 271:1570–1573.

Chen M., El Goresy A., and Gillet P. 2004. Ringwoodite lamellae in olivine: Clues to olivine-ringwoodite phase transition mechanisms in shocked meteorites and subducting slabs. *Proceedings of the National Academy of Sciences* 101:15,033–15,037.

El Goresy A., Chen M., Gillet P., and Dubrovinsky L. S. 2000. Shock-induced high-pressure phase transition of labradorite to hollandite "(Na_{47}-Ca_{51}-K_2)" in Zagami and the assemblage hollandite "(Na_{80}-Ca_{12}-K_8)" + jadeite in L chondrites: constraints to peak shock pressures (abstract). *Meteoritics & Planetary Science* 35:A51.

Ferroir T., Beck P., Van de Moortèle B., Bohn M., Reynard B., Simionovici A., El Goresy A., and Gillet P. 2008. Akimotoite in the Tenham meteorite: Crystal chemistry and high-pressure transformation mechanisms. *Earth and Planetary Science Letters* 275:26–31.

Gillet P., Chen M., Dubrovinsky L., and El Goresy A. 2000. Natural $NaAlSi_3O_8$-hollandite in the shocked Sixiangkou meteorite. *Science* 287:1633–1636.

Gillet P., El Goresy A., Beck P., and Chen M. 2007. High-pressure mineral assemblages in shocked meteorites and shocked terrestrial rocks: Mechanisms of phase transformations and constraints to pressure and temperature histories. In *Advances in high-pressure mineralogy*, edited by Ohtani E. Boulder: The Geological Society of America. pp. 57–82.

Grossman J. N. 1999. The Meteoritical Bulletin, No. 83, 1999 July. *Meteoritics & Planetary Science* 34:A169–A186.

Hogrefe A., Rubie D. C., Sharp T. G., and Seifert F. 1994. Metastability of enstatite in deep subducting lithosphere. *Nature* 372:351–353.

Ito E. and Takahashi E. 1989. Post-spinel transformations in the system Mg_2SiO_4-Fe_2SiO_4 and some geophysical implications. *Journal of Geophysical Research* 94:10,637–10,646.

James O. B. 1969. Jadeite: Shock-induced formation from oligoclase, Ries crater, Germany. *Science* 165:1005–1008.

Karato S., Riedel M. R., and Yuen D. A. 2001. Rheological structure and deformation of subducted slabs in the mantle transition zone: Implications for mantle circulation and deep earthquakes. *Physics of the Earth and Planetary Interiors* 127:83–108.

Katsura T. and Ito E. 1989. The system Mg_2SiO_4-Fe_2SiO_4 at high pressures and temperatures: Precise determination of stabilities of olivine, modified spinel, and spinel. *Journal of Geophysical Research* 94:15,663–15,670.

Kerschhofer L., Sharp T. G., and Rubie D. C. 1996. Intracrystalline transformation of olivine to wadsleyite and ringwoodite under subduction zone conditions. *Science* 274:79–81.

Kerschhofer L., Rubie D. C., Sharp T. G., McConnell J. D. C., and Dupas-Bruzek C. 2000. Kinetics of intracrystalline olivine-ringwoodite transformation. *Physics of the Earth and Planetary Interiors* 121:59–76.

Kimura M., Suzuki A., Kondo T., Ohtani E., and El Goresy A. 2000. Natural occurrence of high-pressure phases jadeite, hollandite, wadsleyite, and majorite-pyrope garnet in an H chondrite, Yamato 75100. *Meteoritics & Planetary Science* 35:A87–A88.

Kirby S. H., Stein S., Okal E. A., and Rubie D. C. 1996. Metastable mantle phase transformations and deep earthquakes in subducting oceanic lithosphere. *Reviews in Geophysics* 34:261–306.

Kubo T., Ohtani E., Kato T., Shinmei T., and Fujino K. 1998. Effects of water on the α-β transformation kinetics in San Carlos olivine. *Science* 281:85–87.

Kubo T., Ohtani E., and Funakoshi K. 2004. Nucleation and growth kinetics of the α-β transformation in Mg_2SiO_4 determined by in situ synchrotron powder X-ray diffraction. *American Mineralogist* 89:285–293.

Kubo T., Kimura M., Nishi M., Tominaga A., Kato T., Kikegawa T., Funakoshi K., and Miyahara M. 2008. Formation of jadeite from plagioclase: Constraints on the P-T-t conditions of shocked meteorites. *Meteoritics & Planetary Science* 43:A82.

Liu L. 1978. High-pressure phase transformations of albite, jadeite and nepheline. *Earth and Planetary Science Letters* 37:438–444.

Madon M. and Poirier J. P. 1983. Transmission electron microscope observation of α, β and γ $(Mg, Fe)_2SiO_4$ in shocked meteorites: Planar defects and polymorphic transitions. *Physics of the Earth and Planetary Interiors* 33:31–44.

Malavergne V., Guyot F., Benzerara K., and Martinez I. 2001. Description of new shock-induced phases in the Shergotty, Zagami, Nakhla, and Chassigny meteorites. *Meteoritics & Planetary Science* 36:1297–1305.

Melosh H. J. 1989. *Impact cratering: A geological process*. New York: Oxford University Press. 256 p.

Miyahara M., El Goresy A., Ohtani E., Nagase T., Nishijima M., Vashaei Z., Ferroir T., Gillet P., Dubrovinsky L., and Simionovici A. 2008. Evidence for fractional crystallization of wadsleyite and ringwoodite from olivine melts in chondrules entrained in shock-melt veins. *Proceedings of the National Academy of Sciences* 105:8542–8547.

Mosenfelder J. L., Connolly J. A. D., Rubie D. C., and Liu M. 2000. Strength of $(Mg,Fe)_2SiO_4$ wadsleyite determined by relaxation of transformation stress. *Physics of the Earth and Planetary Interiors* 120:63–78.

Mosenfelder J. L., Marton F. C., Ross II C. R., Kerschhofer L., and Rubie D. C. 2001. Experimental constraints on the depth of olivine metastability in subducting lithosphere. *Physics of the Earth and Planetary Interiors* 127:165–180.

Ohtani E., Kagawa N., and Fujino K. 1991. Stability of majorite $(Mg,Fe)SiO_3$ at high pressures and 1800 °C. *Earth and Planetary Science Letters* 102:158–166.

Ohtani E., Kimura Y., Kimura M., Takata T., Kondo T., and Kubo T. 2004. Formation of high-pressure minerals in shocked L6 chondrite Yamato 791384: Constraints on shock conditions and parent body size. *Earth and Planetary Science Letters* 227:505–515.

Price G. D. 1983. The nature and significance of stacking faults in wadsleyite, natural β-$(Mg,Fe)_2SiO_4$ from the Peace River Meteorite. *Physics of the Earth and Planetary Interiors* 33: 137–147.

Price G. D., Putnis A., Angrell S. O., and Smith D. G. W. 1983. Wadsleyite, natural β-$(Mg,Fe)_2SiO_4$ from the Peace River meteorite. *Canadian Mineralogist* 21:29–35.

Putnis A. and Price G. D. 1979. High-pressure $(Mg,Fe)_2SiO_4$ phases in the Tenham chondritic meteorite. *Nature* 280:217–218.

Riedel M. R. and Karato S. 1997. Grain-size evolution in subducted oceanic lithosphere associated with the olivine-spinel transformation and its effects on rheology. *Earth and Planetary Science Letters* 148:27–43.

Rubie D. C. 1984. The olivine-spinel transformation and the rheology of subducting lithosphere. *Nature* 308:505–508.

Rubie D. C. and Ross C. R. 1994. Kinetics of olivine-spinel transformation in subducting lithosphere: Experimental constraints and implications for deep slab processes. *Physics of the Earth and Planetary Interiors* 86:223–241.

Schmitt R. T. 2000. Shock experiments with the H6 chondrite Kernouvé: Pressure calibration of microscopic shock effects. *Meteoritics & Planetary Science* 35:545–560.

Sharp T. G. and DeCarli P. S. 2006. Shock effects in meteorites. In *Meteorites and the early solar system II*, edited by Lauretta D. S. and McSween H. Y. Tucson: The University of Arizona Press. pp. 653–677.

Smith J. V. and Mason B. 1970. Pyroxene-garnet transformation in Coorara meteorite. *Science* 168:832–833.

Stöffler D., Keil K., and Scott E. R. D. 1991. Shock metamorphism of ordinary chondrites. *Geochimica et Cosmochimica Acta* 55: 3845–3867.

Sung C. M. and Burns R. G. 1976. Kinetics of high pressure phase transitions: implications to the evolution of the olivine-spinel transition in the downgoing lithosphere and its consequences on the dynamics of the mantle. *Tectonophysics* 31:1–32.

Tomioka N. 2007. A model for the shear mechanism in the enstatite-akimotoite phase transition. *Journal of Mineralogical and Petrological Sciences* 102:226–232.

Tomioka N. and Fujino K. 1997. Natural $(Mg,Fe)SiO_3$-ilmenite and perovskite in the Tenham meteorite. *Science* 277:1084–1086.

Tomioka N. and Fujino K. 1999. Akimotoite, $(Mg,Fe)SiO_3$, a new silicate mineral of the ilmenite group in the Tenham chondrite. *American Mineralogist* 84:267–271.

Tomioka N., Mori H., and Fujino K. 2000. Shock-induced transition of $NaAlSi_3O_8$ feldspar into a hollandite structure in a L6 chondrite. *Geophysical Research Letters* 27:3997–4000.

Tutti F. 2007. Formation of end-member $NaAlSi_3O_8$ hollandite-type

structure (lingunite) in diamond anvil cell. *Physics of the Earth and Planetary Interiors* 161:143–149.

Xie X., Chen M., Dai C., El Goresy A., and Gillet P. 2001a. A comparative study of naturally and experimentally shocked chondrites. *Earth and Planetary Science Letters* 187:345–356.

Xie X., Chen M., and Wang D. 2001b. Shock-related mineralogical features and P-T history of the Suizhou L6 chondrite. *European Journal of Mineralogy* 13:1177–1190.

Xie Z. and Sharp T. G. 2004. High-pressure phases in shock-induced melt veins of Umbarger L6 chondrite: Constraints of shock pressure. *Meteoritics & Planetary Science* 39:2043–2054.

Xie Z. and Sharp T. G. 2007. Host rock solid-state transformation in a shock-induced melt veins of Tenham L6 chondrite. *Earth and Planetary Science Letters* 254:433–445.

Xie Z., Sharp T. G., and DeCarli P. S. 2006. High-pressure phases in a shock-induced melt vein of the Tenham L6 chondrite: Constraints on shock pressure and duration. *Geochimica et Cosmochimica Acta* 70:504–515.

Yagi A., Suzuki T., and Akaogi M. 1994. High pressure transitions in the system $KAlSi_3O_8$-$NaAlSi_3O_8$. *Physics and Chemistry of Minerals* 21:12–17.

Yanai K. and Kojima H. 1995. *Catalog of Antarctic meteorites*. Tokyo: National Institute of Polar Research. 230 p.

Zhang J. and Herzberg C. 1994. Melting experiments on anhydrous peridotite KLB-1 from 5.0 to 22.5 GPa. *Journal of Geophysical Research* 99:17,729–17,742.

Zhang A., Hsu W., Wang R., and Ding M. 2006. Pyroxene polymorphs in melt veins of the heavily shocked Sixiangkou L6 chondrite. *European Journal of Mineralogy* 18:719–726.